2013 American Control Conference (ACC)
Washington, DC, USA, June 17-19, 2013

Identification of Hammerstein Systems Using Input Amplitude Multiplexing

Benjamin J. Coffer[1], Khaled Aljanaideh[1], and Dennis S. Bernstein[2]

Abstract— **An amplitude multiplexing technique for identifying Hammerstein systems with static nonlinearities is presented in this paper. The input signal to the Hammerstein system is amplitude multiplexed, and the output of the Hammerstein nonlinearity is approximated by a continuous piecewise affine function. The Hammerstein nonlinearity is assumed to pass through the origin. Using this identification technique, we show that, in the presence of zero-mean, colored output noise, the estimates of the Hammerstein nonlinearity and the impulse response of the linear plant are asymptotically correct up to a scalar factor.**

I. Introduction

Hammerstein systems extend the class of linear systems by cascading the linear system with an input nonlinearity. The input nonlinearity may be static, as in the case of magnitude saturation, deadzone, and signum nonlinearities, or it may be dynamic, as in the case of rate saturation or hysteresis. As these examples suggest, Hammerstein systems arise in virtually all practical applications of control.

In view of their widespread application, extensive effort has been devoted to identifying Hammerstein systems [1–10]. In the most extreme case, the input nonlinearity may be unknown, and the objective is to identify both the linear system dynamics and the input nonlinearity. In some applications, partial information about the input nonlinearity may be available; for example, the input nonlinearity may be assumed to be odd or its value at zero may be assumed to be known or zero. The techniques used to identify Hammerstein systems typically rely on least squares optimization.

In the present paper, we develop a novel amplitude-multiplexing technique for identifying Hammerstein systems with static input nonlinearities. This technique replaces the input to the Hammerstein system by a collection of signals obtained by passing the input through multiple saturation functions whose lower and upper limits partition the range of the input. Each resulting saturated signal is then shifted so that the minimum of its absolute value is zero. The input nonlinearity is then approximated by a linear combination of the amplitude-multiplexed signals. By applying least squares optimization, we thus obtain a piecewise-linear approximation of the input nonlinearity.

A widely used approach to identifying Hammerstein systems is to approximate the input nonlinearity by a linear combination of basis functions [11, 12]. Since these basis functions are known, the scalar control input can be replaced by a vector of control "inputs," whose components are the basis functions evaluated at each value of the control input. This leads to a MISO linear identification problem. An estimate of the input matrix of the nonlinear system is obtained through a singular value decomposition of the input matrix estimated for the MISO system. The amplitude-multiplexing approach of the present paper is based on a choice of basis functions that leads directly to a continuous, piecewise-affine approximation of the input nonlinearity. This technique thus provides an alternative approach to the continuous, piecewise-affine approximation approach to Hammerstein system identification given in [10].

The contents of the paper are as follows. In section II we formulate the problem. In section III we show the identification technique. Numerical examples are presented in section IV. We give conclusions in section V.

II. Problem Formulation

Consider the discrete-time SISO Hammerstein system shown in Figure 1, where u is the input, $f : \mathbb{R} \to \mathbb{R}$ is a static nonlinearity, $f(u)$ is the intermediate signal, and y is the output of the asymptotically stable, SISO, linear, time-invariant, discrete-time system G. In the following we describe a novel identification algorithm where the nonlinearity f and the impulse response of the plant G are estimated given measurements of the input u and output y.

First, we amplitude multiplex the single input u into n sub-inputs u_1, u_2, …, u_n as shown in Figure 2. As Figure 2 illustrates, u is partitioned horizontally at s_1, s_2, …, s_{n+1}. The signals u_1, u_2, …, u_n are then generated by saturation from the regions between partitions. For example, u_4 is generated by saturating u between s_4 and s_5 and then subtracting s_4 so that the minimum value of u_4 is zero. Negative-valued partitions are handled differently. For example, u_1 is generated by saturating u between s_1 and s_2 and then subtracting s_2 such that the *maximum* value of u_1 is zero. Specifically, we define the amplitude-multiplexing function

$$\mathcal{M}(u(k)) \triangleq \begin{bmatrix} u_1(k) & \cdots & u_n(k) \end{bmatrix} \in \mathbb{R}^{1\times n}, \qquad (1)$$

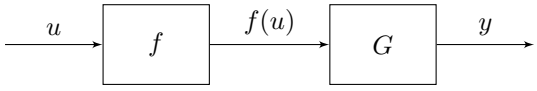

Fig. 1. SISO Hammerstein System. u is the input, f represents a static nonlinearity, $f(u)$ is the intermediate signal, and y is the output of the linear, time-invariant, discrete-time system G.

[1] Graduate student, Department of Aerospace Engineering, The University of Michigan, Ann Arbor, MI 48109.

[2] Professor, Department of Aerospace Engineering, The University of Michigan, Ann Arbor, MI 48109.

978-1-4799-0176-0/$31.00 ©2013 AACC

where

$$u_i(k) \triangleq \text{sat}_{[s_i,\ s_{i+1}]}(u(k)) - \begin{cases} s_i & \text{if } s_i \geq 0, \\ s_{i+1} & \text{if } s_i < 0, \end{cases} \tag{2}$$

and the saturation function is defined by

$$\text{sat}_{[a,\ b]}(x) \triangleq \begin{cases} a & \text{if } x < a, \\ x & \text{if } a \leq x \leq b, \\ b & \text{if } x > b. \end{cases} \tag{3}$$

We require that the partition values be increasing, that is, $s_1 < s_2 < \cdots < s_{n+1}$, and that one of the partition values be zero. If necessary, the input can be shifted by defining $v \triangleq u+b$ for some constant b and then applying the identification method to v and y. Furthermore, the input signal u must be contained within all partitions, that is, $s_1 \leq u(k) \leq s_{n+1}$ for all $k \geq 0$. Finally, each sub-input u_p must be persistently exciting. If this is not the case, singularity problems can arise.

We assume that G is represented by an FIR model as

$$G(\mathbf{q}) = \frac{B(\mathbf{q})}{A(\mathbf{q})}, \tag{4}$$

where $A(\mathbf{q}) = \mathbf{q}^\mu$ and $B(\mathbf{q}) = \sum_{i=0}^{\mu} H_i \mathbf{q}^i$, H_i is the i^{th} FIR Markov (impulse response) parameter of G, and μ is the model order. Moreover, we assume that f can be approximated by a continuous piecewise-affine function defined by

$$\hat{f}(u) \triangleq \mathcal{M}(u)\ \alpha_n, \tag{5}$$

where

$$\alpha_n \triangleq \begin{bmatrix} a_1 & \cdots & a_n \end{bmatrix}^{\mathrm{T}}, \tag{6}$$

is unknown. As illustrated in Figure 3, a_i is the slope of $\hat{f}(u)$ between the partition values s_i, s_{i+1}, for all $i \in \{1, \ldots, n\}$.

Define

$$e_f(u) \triangleq f(u) - \hat{f}(u) \tag{7}$$

to be the difference between the actual and the approximated intermediate signals. If e_f tends to zero, then $\hat{f}(u)$ tends to $f(u)$.

Define the vector of Markov parameters

$$\theta_\mu \triangleq \begin{bmatrix} H_0 & \cdots & H_\mu \end{bmatrix}. \tag{8}$$

In this paper we aim to estimate θ_μ and the vector of coefficients α_n given the input u and the output y.

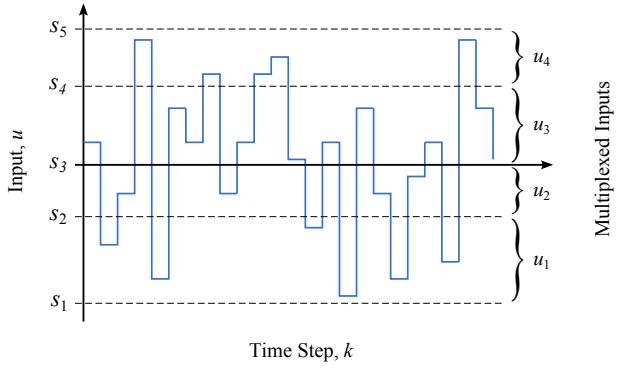

Fig. 2. Illustration of amplitude multiplexing of the input u to obtain multiple inputs $u_1, \ldots, u_n$. In this illustration, $n = 4$ and $s_3 = 0$.

III. Estimation of f and θ_μ

We assume here that the Hammerstein nonlinearity passes through the origin, that is, $f(0) = 0$.

Consider the block diagram in Figure 4, where u is the input, y_0 is the output, and w is the output noise. We assume no input noise and w is zero-mean colored noise independent of u. The signal y represents the measurement of the output y_0, that is,

$$y = y_0 + w. \tag{9}$$

Let m denote the number of measurements of u and y. Define

$$U \triangleq \begin{bmatrix} \mathcal{M}(u(1)) \\ \vdots \\ \mathcal{M}(u(m)) \end{bmatrix} \in \mathbb{R}^{m \times n}, \tag{10}$$

which allows us to write the approximated intermediate signal as

$$\hat{f}(u(k)) = \mathcal{M}(u(k))\alpha_n = \sum_{i=1}^{n} a_i u_i(k). \tag{11}$$

Next, note that the output $y_0(k)$ of the Hammerstein system at time k, can be approximated by $\hat{y}_0(k)$, where

$$\begin{aligned} \hat{y}_0(k) &= \sum_{i=0}^{\mu} H_i \hat{f}(u(k-i)) \\ &= \sum_{i=0}^{\mu} H_i \mathcal{M}(u(k-i))\alpha_n. \end{aligned} \tag{12}$$

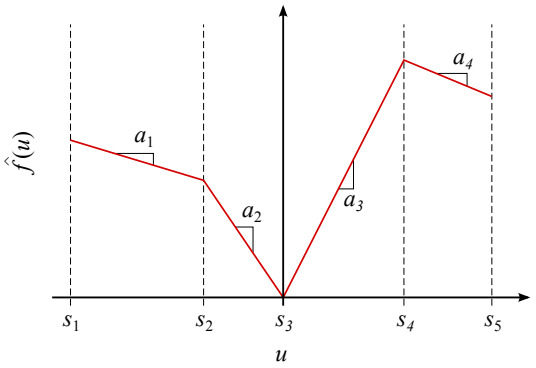

Fig. 3. Illustration of the approximate nonlinear function $\hat{f}(u)$. The coefficients $a_1, \ldots, a_n$ are the slopes of the line segments between partitions. In this illustration, $n = 4$ and $s_3 = 0$.

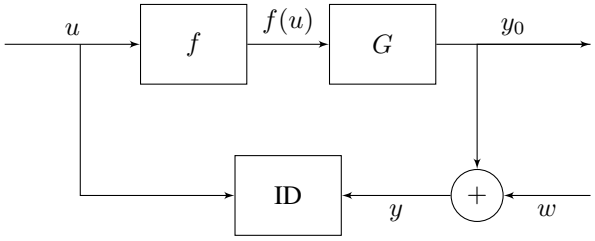

Fig. 4. Identification of the Hammerstein system (f, G). u and y_0 represent input and output signals, respectively, where w represents output noise.

Define the difference between y_0 and $\hat{y}_0$ at time k to be

$$e_y(k) \stackrel{\triangle}{=} y_0(k) - \hat{y}_0(k). \tag{13}$$

Therefore, the output $y_0(k)$ can be written as

$$\begin{aligned} y_0(k) &= \sum_{i=0}^{\mu} \mathcal{M}(u(k-i))\alpha_n H_i + e_y(k) \\ &= \phi_\mu(k)\gamma_{n,\mu} + e_y(k), \end{aligned} \tag{14}$$

where

$$\phi_\mu(k) \stackrel{\triangle}{=} \left[\begin{array}{ccc} \mathcal{M}(u(k)) & \cdots & \mathcal{M}(u(k-\mu)) \end{array} \right] \in \mathbb{R}^{1\times n(\mu+1)},$$
$$\gamma_{n,\mu} \stackrel{\triangle}{=} \mathrm{vec}\,(\alpha_{\mathrm{n}}\theta_\mu) \in \mathbb{R}^{\mathrm{n}(\mu+1)\times 1}.$$

It follows that

$$\Psi_{y,m} = \Phi_{\mu,m}\gamma_{n,\mu} + \Psi_{w,m} + \Psi_{e_y,m}, \tag{15}$$

where

$$\begin{aligned} \Psi_{y,m} &\stackrel{\triangle}{=} \left[\begin{array}{ccc} y(\mu) & \cdots & y(m) \end{array} \right]^{\mathrm{T}} \in \mathbb{R}^{(m-\mu+1)\times 1}, \\ \Phi_{\mu,m} &\stackrel{\triangle}{=} \left[\begin{array}{ccc} \phi_\mu^{\mathrm{T}}(\mu) & \cdots & \phi_\mu^{\mathrm{T}}(m) \end{array} \right]^{\mathrm{T}} \in \mathbb{R}^{(m-\mu+1)\times n(\mu+1)}, \\ \Psi_{w,m} &\stackrel{\triangle}{=} \left[\begin{array}{ccc} w(\mu) & \cdots & w(m) \end{array} \right]^{\mathrm{T}} \in \mathbb{R}^{(m-\mu+1)\times 1}, \\ \Psi_{e_y,m} &\stackrel{\triangle}{=} \left[\begin{array}{ccc} e_y(\mu) & \cdots & e_y(m) \end{array} \right]^{\mathrm{T}} \in \mathbb{R}^{(m-\mu+1)\times 1}. \end{aligned}$$

The least squares estimate $\hat{\gamma}_{n,\mu,m}$ of $\gamma_{n,\mu}$ is given by

$$\hat{\gamma}_{n,\mu,m} = \arg\min_{\bar{\gamma}_{n,\mu}} \left\| \Psi_{y,m} - \Phi_{\mu,m}\bar{\gamma}_{n,\mu} \right\|_{\mathrm{F}}, \tag{16}$$

where $\bar{\gamma}_{n,\mu} \in \mathbb{R}^{n(\mu+1)\times 1}$, and $||\ .\ ||_{\mathrm{F}}$ denotes the Frobenius norm. It follows from (16) that

$$\Phi_{\mu,m}^{\mathrm{T}}\Psi_{y,m} = \Phi_{\mu,m}^{\mathrm{T}}\Phi_{\mu,m}\hat{\gamma}_{n,\mu,m}, \tag{17}$$

that is,

$$\Phi_{\mu,m}^{\mathrm{T}}\left[\Psi_{\hat{y}_0,m} + \Psi_{w,m} + \Psi_{e_y,m}\right] = \Phi_{\mu,m}^{\mathrm{T}}\Phi_{\mu,m}\hat{\gamma}_{n,\mu,m}, \tag{18}$$

where

$$\begin{aligned} \Psi_{\hat{y}_0,m} &\stackrel{\triangle}{=} \left[\begin{array}{ccc} \hat{y}_0(\mu) & \cdots & \hat{y}_0(m) \end{array} \right]^{\mathrm{T}} \in \mathbb{R}^{(m-\mu+1)\times 1}, \\ \Psi_{e_y,m} &\stackrel{\triangle}{=} \left[\begin{array}{ccc} e_y(\mu) & \cdots & e_y(m) \end{array} \right]^{\mathrm{T}} \in \mathbb{R}^{(m-\mu+1)\times 1}. \end{aligned}$$

Dividing (18) by m and taking the limit yields,

$$\lim_{m\to\infty} \frac{1}{m}\Phi_{\mu,m}^{\mathrm{T}}\left[\Phi_{\mu,m}\gamma_{n,\mu} + \Psi_{w,m} + \Psi_{e_y,m}\right] = \lim_{m\to\infty} \frac{1}{m}\Phi_{\mu,m}^{\mathrm{T}}\Phi_{\mu,m}\hat{\gamma}_{n,\mu,m}. \tag{19}$$

Note that,

$$\lim_{m\to\infty} \frac{1}{m}\Phi_{\mu,m}^{\mathrm{T}}\Psi_{w,m} \stackrel{\mathrm{wp1}}{=} 0_{n(\mu+1)\times 1}. \tag{20}$$

Moreover, suppose that we choose n such that $\lim_{m\to\infty}\Psi_{e_y,m}$ is negligible for all $k \geq 0$. It follows from (19) that

$$\lim_{m\to\infty} \frac{1}{m}\Phi_{\mu,m}^{\mathrm{T}}\Phi_{\mu,m}\gamma_{n,\mu} \stackrel{\mathrm{wp1}}{=} \lim_{m\to\infty} \frac{1}{m}\Phi_{\mu,m}^{\mathrm{T}}\Phi_{\mu,m}\hat{\gamma}_{n,\mu,m}, \tag{21}$$

that is,

$$\lim_{m\to\infty} \hat{\gamma}_{n,\mu,m} \stackrel{\mathrm{wp1}}{=} \gamma_{n,\mu}. \tag{22}$$

Define

$$\Gamma \stackrel{\triangle}{=} (\alpha_n\theta_\mu)^{\mathrm{T}} \in \mathbb{R}^{(\mu+1)\times n},$$

and note that the rank of Γ is 1. Moreover, Γ can be written as

$$\Gamma = \left[\begin{array}{ccc} \Gamma_1 & \cdots & \Gamma_n \end{array} \right], \tag{23}$$

where

$$\Gamma_i \stackrel{\triangle}{=} a_i\theta_\mu^{\mathrm{T}}, \tag{24}$$

for $i = 1, \ldots, n$. Note that,

$$\gamma_{n,\mu} = \mathrm{vec}(\Gamma^{\mathrm{T}}). \tag{25}$$

To obtain α_n from Γ, note that

$$\frac{\Gamma_i}{a_i} = \frac{\Gamma_j}{a_j}, \tag{26}$$

for all $i, j \in \{1, \ldots, n\}$. That is,

$$\Gamma_i = \frac{a_i}{a_j}\Gamma_j. \tag{27}$$

Solving the over-constrained linear equation (27) in a least-squares sense yields

$$\frac{a_i}{a_j} = \frac{\Gamma_j^{\mathrm{T}}\Gamma_i}{\Gamma_j^{\mathrm{T}}\Gamma_j}, \tag{28}$$

for all $i, j \in \{1, \ldots, n\}$. We then note that

$$\begin{aligned} \Gamma^{\mathrm{T}}\Gamma\alpha_n &= (\alpha_n\theta_\mu)(\alpha_n\theta_\mu)^{\mathrm{T}}\alpha_n \\ &= \left(\sum_{i=0}^{\mu} H_i^2 \sum_{j=1}^{n} a_j^2\right)\alpha_n, \\ &= \lambda\alpha_n, \end{aligned} \tag{29}$$

where

$$\lambda \stackrel{\triangle}{=} \sum_{i=0}^{\mu} H_i^2 \sum_{j=1}^{n} a_j^2 \in \mathbb{R}. \tag{30}$$

Note from (29) that α_n is an eigenvector of the matrix $\Gamma^{\mathrm{T}}\Gamma$, then for any nonzero $\beta \in \mathbb{R}$, $\beta\alpha_n$ is also an eigenvector of $\Gamma^{\mathrm{T}}\Gamma$, and $\beta\lambda$ is the eigenvalue that corresponds to the eigenvector $\beta\alpha_n$. Moreover, since $\mathrm{rank}(\Gamma) = 1$, it follows that $\mathrm{rank}(\Gamma^{\mathrm{T}}\Gamma) = 1$, therefore, $\beta\alpha_n$ is the eigenvector of $\Gamma^{\mathrm{T}}\Gamma$ that corresponds to the only nonzero (i.e. the biggest) eigenvalue, which is $\beta\lambda$.

Finally, once $\beta\alpha_n$ has been obtained, we can obtain θ_μ using the averaging equation,

$$\theta_\mu = \frac{(|\beta a_1| + \cdots + |\beta a_n|)\theta_\mu}{(|\beta a_1| + \cdots + |\beta a_n|)} \tag{31}$$

$$= \beta\frac{\mathrm{sgn}(\beta a_1)\Gamma_1 + \cdots + \mathrm{sgn}(\beta a_n)\Gamma_n}{|\beta a_1| + \cdots + |\beta a_n|}. \tag{32}$$

Note from (32) that the vector of Markov parameters is identified up to a scalar factor.

IV. Numerical Examples

In this section we show examples with odd, even, and neither odd nor even nonlinearities for both cases of smooth and nonsmooth nonlinearities. Let u be a realization of the uniformly distributed random process $\mathcal{U}$ with the probability density function

$$p(u) = \begin{cases} \frac{1}{2a}, & |u| \leq a, \\ 0, & |u| > a. \end{cases} \tag{33}$$

To show that the estimated nonlinearity and impulse response are asymptotically correct up to a scalar factor β, in each of the following examples we plot the actual nonlinearity and impulse response and the estimated nonlinearity and impulse response after modifying them using the correct scalar β.

Example 4.1: Consider the Hammerstein system

$$f(u) = u^3, \tag{34}$$

$$G = \frac{-3z^2 - 1.2z + 0.5}{z^3 + 1.2z^2 + 0.28z - 1}. \tag{35}$$

Let $\mathcal{U}$ be white and have the uniform pdf (33) with $a = 3$. We set $m = 10,000$, $\mu = 40$, $n = 6$, and the partition values $s_1 = -\infty, s_2 = -2, s_3 = -1, s_4 = 0, s_5 = 1, s_6 = 2, s_7 = +\infty$. In this example we use noise-free data. Figure 5 shows the actual and estimated nonlinearities and Figure 6 shows the actual and estimated Markov parameters of G. Note that the estimation is close for both of the nonlinearity and the Markov parameters.

Example 4.2: Consider the Hammerstein system

$$f(u) = u^2 \tag{36}$$

$$G = \frac{0.7z^4 + 2.6z^3 + 4z^2 + 2z - 2.5}{z^4 + 0.4z^3 + 0.43z^2 + 0.5z + 0.05}. \tag{37}$$

Let $\mathcal{U}$ be white and have the uniform pdf (33) with $a = 3$. We set $m = 10,000$, $\mu = 40$, $n = 60$, and the partition values $s_p = -3, -2.9, -2.8, \ldots, 2.8, 2.9, 3$, for $p = 1, 2, 3, \ldots, 59, 60, 61$, respectively. In this example we use noise-free data. Figure 7 shows the actual and estimated nonlinearities and Figure 8 shows the actual and estimated Markov parameters of G. Note that the estimation is close for both of the nonlinearity and the Markov parameters.

Example 4.3: Consider the Hammerstein system

$$f(u) = 10\sin(u^2) + u^3 \tag{38}$$

$$G = \frac{1.3z^3 + 0.13z^2 - 2.28z - 1.27}{z^5 - 0.5z^4 + 0.46z^3 - 0.17z^2 - 0.16z - 0.02}. \tag{39}$$

Let $\mathcal{U}$ be white and have the uniform pdf (33) with $a = 3$. We set $m = 10,000$, $\mu = 40$, $n = 60$, and the partition values $s_p = -3, -2.9, -2.8, \ldots, 2.8, 2.9, 3$, for $p = 1, 2, 3, \ldots, 59, 60, 61$, respectively. In this example we use noise-free data. Figure 9 shows the actual and estimated nonlinearities and Figure 10 shows the actual and estimated Markov parameters of G. Note that the estimation is close for both of the nonlinearity and the Markov parameters.

Example 4.4: In this example we repeat Example 4.3 using output noise with SNR of 4. Figure 11 shows the actual and estimated nonlinearities and Figure 12 shows the actual and estimated Markov parameters of G. Note that the estimation is close for both of the nonlinearity and the Markov parameters.

Example 4.5: Consider the Hammerstein system

$$G = \frac{1.1z^2 - 0.33z - 0.31}{z^3 + 0.1z^2 + 0.35z - 0.33}. \tag{40}$$

and $f(u)$ is a deadzone nonlinearity which begins at -0.504 and ends at 0.5. Let $\mathcal{U}$ be white and have the uniform pdf (33) with $a = 3$. We set $m = 10,000$, $\mu = 40$, $n = 60$, and the partition values $s_p = -3, -2.9, -2.8, \ldots, 2.8, 2.9, 3$, for $p = 1, 2, 3, \ldots, 59, 60, 61$, respectively. In this example we use noise-free data. Figure 13 shows the actual and estimated nonlinearities and Figure 14 shows the actual and estimated Markov parameters of G. Note that the estimation is close for both of the nonlinearity and the Markov parameters.

Example 4.6: Consider the Hammerstein system where,

$$G = \frac{1.1z^3 - 0.22z^2 - 1.75z + 1}{z^3 - 0.6z^2 - 0.54z + 0.46}. \tag{41}$$

and the nonlinearity $f(u)$ is a square wave as shown in Figure 15. Let $\mathcal{U}$ be white and have the uniform pdf (33) with $a = 3$. We set $m = 10,000$, $\mu = 40$, $n = 60$, and the partition values $s_p = -3, -2.9, -2.8, \ldots, 2.8, 2.9, 3$, for $p = 1, 2, 3, \ldots, 59, 60, 61$, respectively. In this example we

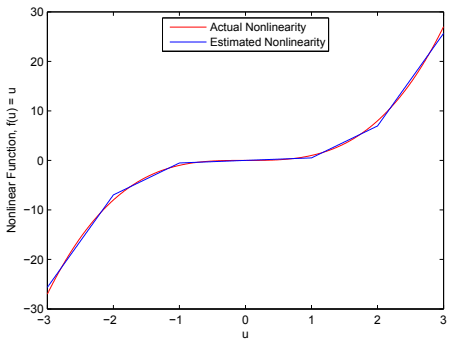

Fig. 5. Actual and estimated nonlinearities for Example 4.1, where $f(u) = u^3$. Note that the estimated and actual nonlinearities are close to each other.

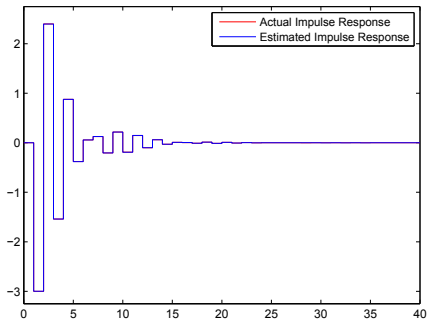

Fig. 6. Actual and estimated Markov parameters of G for Example 4.1, where $G(z)$ as given in (35). Note that the estimated and actual Markov parameters are close to each other.

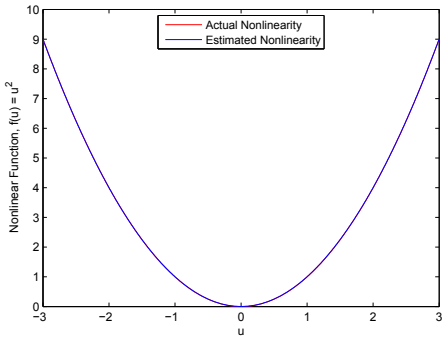

Fig. 7. Actual and estimated nonlinearities for Example 4.2, where $f(u) = u^2$. Note that the estimated and actual nonlinearities are close to each other.

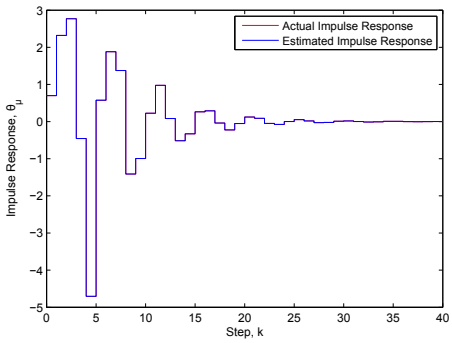

Fig. 8. Actual and estimated Markov parameters of G for Example 4.2, where $G(z)$ as given in (37). Note that the estimated and actual Markov parameters are close to each other.

use noise-free data. Figure 15 shows the actual and estimated nonlinearities and Figure 16 shows the actual and estimated Markov parameters of G. Note that the estimation is close for both of the nonlinearity and the Markov parameters.

V. Conclusions

In this paper we introduced a novel amplitude multiplexing technique for identifying Hammerstein systems with static nonlinearities that pass through the origin. The input to the Hammerstein system was replaced by a collection of signals obtained by passing the input through multiple saturation

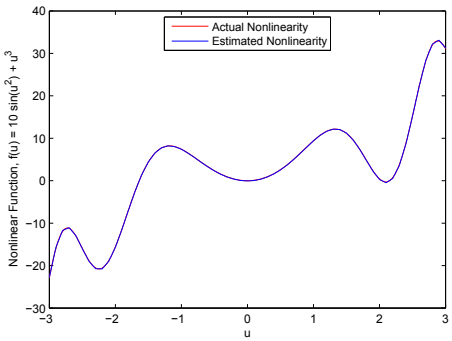

Fig. 9. Actual and estimated nonlinearities for Example 4.3, where $f(u) = 10\sin(u^2) + u^3$. Note that the estimated and actual nonlinearities are close to each other.

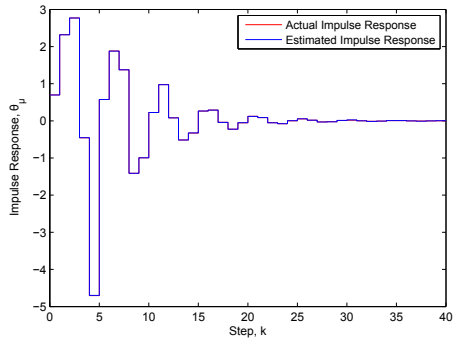

Fig. 10. Actual and estimated Markov parameters of G for Example 4.3, where $G(z)$ as given in (39). Note that the estimated and actual Markov parameters are close to each other.

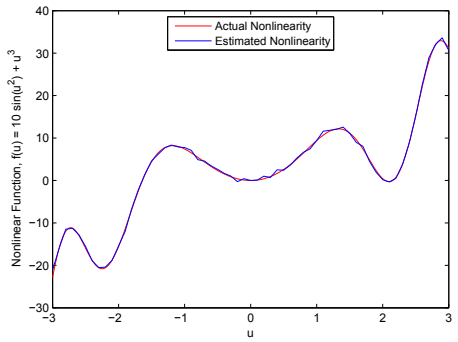

Fig. 11. Actual and estimated nonlinearities for Example 4.4, where $f(u) = 10\sin(u^2) + u^3$ and output SNR is 4. Note that the estimated and actual nonlinearities are close to each other. Comparing Figure 9 with shows the effect of noise.

functions whose lower and upper limits partition the range of the input. Moreover, the output of the Hammerstein nonlinearity was approximated by a continuous piecewise linear function. Using the identification technique presented in this paper, we showed that the estimates of the Hammerstein nonlinearity and the impulse response of the linear plant were asymptotically correct up to a scalar factor. We showed different examples including even, odd, and neither even nor odd nonlinearities for both cases of smooth and non-smooth nonlinearities.

References

[1] A. A. Ali, A. M. D'Amato, M. S. Holzel, S. L. Kukreja, and D. S. Bernstein, "Consistent identification of hammerstein systems using an ersatz nonlinearity," in *Proc. Amer. Contr. Conf.*, San Francisco, CA, July 2011, pp. 1242–1246.

[2] W. Greblicki and M. Pawlak, "Identification of discrete Hammerstein systems using kernel regression estimates," vol. AC-31, 1986, pp. 74–77.

[3] P. Crama and J. Schoukens, "Initial estimates of wiener and hammerstein systems using multisine excitation," *IEEE Trans. Instrum. Meas.*, vol. 50, no. 6, pp. 1791–1795, 2001.

[4] C. Chen and S. D. Fassois, "Maximum liklihood identifiation of stochastic wiener-hammerstein-type nonlinear-systems." *Mechanical Systems and Signal Processing*, vol. 6, no. 2, pp. 135–153, 1992.

[5] X. Hong and R. Mitchell, "Hammerstein model identification algorithm using bezier-bernstein approximation." *Control Theory and Applications, IET*, vol. 1, no. 4, pp. 1149–1159, 2007.

[6] J. S. P. Crama, "Hammersteinwiener system estimator initialization." *Automatica*, vol. 39, pp. 1543–1550, 2004.

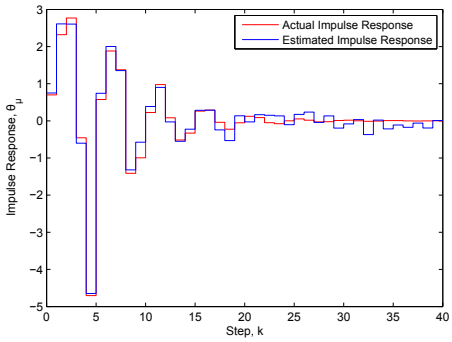

Fig. 12. Actual and estimated Markov parameters of G for Example 4.4, where $G(z)$ as given in (39) and output SNR is 4. Note that the estimated and actual Markov parameters are close to each other. Compare with Figure 10 to note the effect of noise

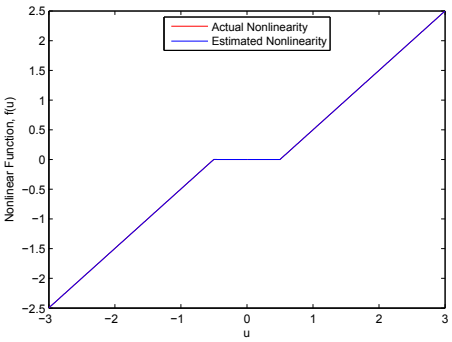

Fig. 13. Actual and estimated nonlinearities for the dead-zone nonlinearity $f(u)$ in Example 4.5. Note that the estimated and actual nonlinearities are close to each other.

[7] F. Z. Chaoui, F. Giri, Y. Rochdi, M. Haloua, and A. Naitali, "System identification based on hammerstein model," *International J. Contr.*, vol. 78, no. 6, p. 430442, 2005.

[8] E.-W. Bai, "Decoupling the linear and nonlinear parts in hammerstein model identification." *Automatica*, vol. 40, pp. 671–676, 2004.

[9] B. Ninness and S. Gibson, "Quantifying the accuracy of hammerstein model estimation." *Automatica*, vol. 38, pp. 2037–2051, 2002.

[10] T. H. Van Pelt and D. S. Bernstein, "Non-linear system identification using hammerstein and non-linear feedback models with piecewise linear static maps." *International J. Contr.*, vol. 74, no. 18, pp. 1807–1823, 2001.

[11] H. Palanthandalam-Madapusi, J. B. Hoagg, and D. S. Bernstein, "Basis-function optimization for subspace-based nonlinear identification of systems with measured-input nonlinearities." in *Proc. Amer. Contr. Conf.*, Boston, MA, July 2004, pp. 4788–4793.

[12] S. L. Lacy and D. S. Bernstein, "Subspace identification for nonlinear systems with measured-input nonlinearities." *International J. Contr.*, vol. 78, pp. 906–926, 2005.

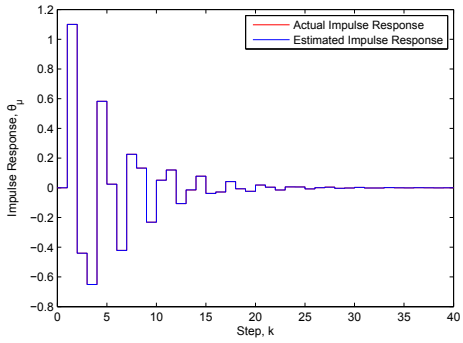

Fig. 14. Actual and estimated Markov parameters of G for Example 4.5, where $G(z)$ as given in (40). Note that the estimated and actual Markov parameters are close to each other.

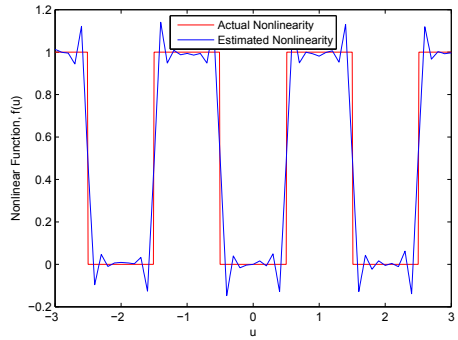

Fig. 15. Actual and estimated nonlinearities for the square wave nonlinearity $f(u)$ from Example 4.6. Note that the estimated and actual nonlinearities are close to each other.

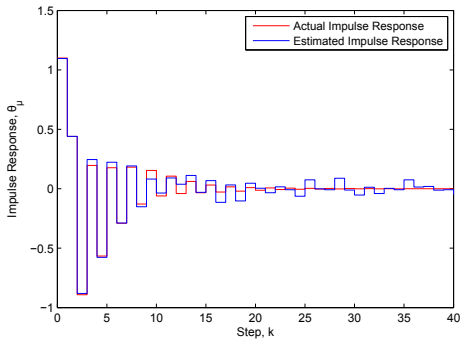

Fig. 16. Actual and estimated Markov parameters of G for Example 4.6, where $G(z)$ as given in (41). Note that the estimated and actual Markov parameters are close to each other.